Distinct higher-order α-synuclein oligomers induce intracellular aggregation

Eva Illes-Toth*[1], Mafalda Ribeiro Ramos*, Roberto Cappai†, Caroline Dalton* and David P Smith*[2]

*Biomedical Research Centre, Sheffield Hallam University, Howard Street, Sheffield S1 1WB, U.K.
†Department of Pathology, Bio21 Molecular Science and Biotechnology Institute, The University of Melbourne, Victoria 3010, Australia

Misfolding and aggregation of α-synuclein (α-syn) into Lewy bodies is associated with a range of neurological disorders, including Parkinson's disease (PD). The cell-to-cell transmission of α-syn pathology has been linked to soluble amyloid oligomer populations that precede Lewy body formation. Oligomers produced *in vitro* under certain conditions have been demonstrated to induce intracellular aggregation in cell culture models. In the present study, we characterize, by ESI–ion mobility spectrometry (IMS)–MS, a specific population of α-syn oligomers. These MS-compatible oligomers were compared with oligomers with known seeding and pore-forming capabilities and were shown to have the ability to induce intracellular aggregation. Each oligomer type was shown to have distinct epitope profiles that correlated with their toxic gain-of-function. Structurally, the MS compatible oligomers populated a range of species from dimers through to hexamers. Lower-order oligomers were structurally diverse and consistent with unstructured assemblies. Higher-order oligomers were shown to be compact with ring-like structures. The observation of this compact state may explain how this natively disordered protein is able to transfer pathology from cell to cell and avoid degradation by cellular proteases.

Key words: α-synuclein, aggregation, amyloid, ion mobility, mass spectrometry (MS), oligomer.

INTRODUCTION

α-Synuclein (α-syn) instigates both sporadic and idiopathic Parkinson's disease (PD) by various modes of action [1] and is the major component of intracellular Lewy bodies and Lewy neurites in the brain [2]. The three rare missense mutations of α-syn (A30P, A53T and E46K), copy number variants and two probable substitutions (H50Q and G51D) are associated with familial PD, indicating a central role for this protein [3]. Growing evidence suggests that soluble oligomeric forms of α-syn, which precede amyloid formation, are causative triggers for the dopaminergic cell loss occurring in PD [4,5]. The morphology and associated mode of toxicity displayed by alternative types of α-syn oligomers are largely dependent on the environmental conditions under which they have been prepared [6–11]. Numerous *in vitro* and *in vivo* studies on α-syn oligomers have demonstrated that a toxic gain-of-function occurs in the disease state via two main mechanisms: (i) Ca^{2+} imbalances caused by the formation of pore-like complexes within lipid membranes, and (ii) transmembrane seeding that then results in intracellular aggregation [1]. α-Syn is expressed as an intracellular protein but has been shown to be directly secreted or released as a result of neuronal death or stress conditions into the extracellular space [12]. Soluble oligomeric forms of α-syn have also been detected in the cerebrospinal fluid and sera of PD patients [13–16].

α-Syn pathology can spread from cell to cell, in both cell culture and *in vivo* models of PD, by exogenously added oligomeric forms which then induce intracellular aggregation and propagation of α-syn in adjacent cells, initiating neuroinflammation [12,17]. Short fragmented α-syn amyloid fibrils have also been reported to trigger endogenous α-syn to aggregate and accumulate sustainably over several passages in non-transfected and transfected SH-SY5Y cells [18]. The morphology and characteristics of intracellular inclusions have been demonstrated to be influenced by the variant of α-syn seed applied. In neurons, astrocytes and mixed primary cells, sonicated A53T fibrils seeded 'flame-like inclusions', whereas small E46K fibrils prompted the formation of punctate round-shaped structures depending on the form of α-syn expressed. In addition, the inclusions could be transferred during passaging in a prion-like manner [19]. Further evidence for the prion-like seeding mechanism of α-syn has arisen from a variety of *in vivo* experimentation at the cellular, intercellular and tissue levels which has been strengthened by sporadic cases of transmission in mesencephalic transplants of PD patients. Although evidence points towards a prion-like transmission of α-syn, improved cellular and animal models and longitudinal studies are essential to make progress in this field of research [20]. Oueslati et al. [21] also highlighted key aspects that have to be explored regarding the sequence-specific homotypic self-templating of α-syn via preformed fibrils or heterotypic seeding of α-syn acting in concert with Aβ peptides or tau. As the addition and uptake of preformed seeds or intracerebral inoculation of brain homogenates have been investigated in culture and transgenic mice, important questions remain to be answered about the initiating steps and course of propagation in the anatomical context of PD. These events are exacerbated by an imbalance of multiple cellular degradation pathways (ubiquitin–proteasome system, autophagy–lysosome pathway and other known proteolytic and cellular enzymes) affecting clearance of misfolded α-syn and concurrent activation of inflammatory responses [21].

The self-assembly of α-syn and the factors that modulate its aggregation, i.e. pH, temperature, post-translational modifications [22], ligands [23] and metals [24,25], have been extensively

studied by a variety of biophysical methods. However, the use of high-resolution biophysical methods, e.g. NMR spectroscopy, in characterizing the heterogeneous soluble amyloidogenic oligomers is hindered due to their low concentrations and transient nature in solution. In contrast, ESI–ion mobility spectrometry (IMS)–MS has unique advantages to determine the mass and conformation of oligomeric assemblies in a rapid time frame using femtomolar protein concentrations [26]. Ion mobility measurements, accompanied by molecular modelling, permit the assignment of possible geometries for unknown protein complexes, and this gives valuable insights into the topology of the oligomers [27,28]. In the present study, oligomeric forms of α-syn [6,29] have been solubilized under MS-compatible conditions by the use of ammonium acetate as a buffer to enable ESI–IMS–MS analysis. Ion mobility experiments and molecular modelling demonstrate that the oligomeric species present encompass dimers to hexamers with various morphologies and suggest that assembly follows an isotropic growth pathway. Higher-order oligomers have collision cross-sectional areas (Ω) consistent with a ring-like assembly. These MS data, in conjunction with cell viability measurements, show that these oligomers lack the ability to induce Ca^{2+} influx, but are able to induce intracellular aggregation in a prion-like manner.

MATERIALS AND METHODS

Preparation of α-syn oligomers

Monomeric α-syn was expressed in *Escherichia coli* and purified as described previously [30]. Oligomer preparation of both seeding- and pore-forming-type oligomers used as positive controls is fully described in the Supplementary Online Data and in [6]. To make the MS-compatible oligomers (i.e. suitable for ESI–IMS–MS analysis), 50 mM sodium phosphate buffer was replaced with 50 mM ammonium acetate, pH 7.0. In protocol 1, α-syn was dissolved at 7 μM in either buffer, containing 20 % ethanol for production of oligomers. After 4 h of incubation, oligomers were lyophilized and resuspended with one-half of starting volume in either buffer containing 10 % ethanol, followed by incubation with agitation for 24 h at 21 °C with open lids to evaporate residual ethanol. Oligomers were then further incubated for 6 days with closed lids at 21 °C. In protocol 2, α-syn was dissolved at 7 μM in 50 mM sodium phosphate buffer, containing 20 % ethanol followed by overnight incubation at 21 °C with continuous shaking, the oligomers were concentrated and separated from monomer using VivaSpin500 30 000 Da molecular-mass cut-off columns (Sartorius).

Biochemical characterization

Procedures for epitope mapping by dot blotting, immuno-cytochemistry, Ca^{2+} influx assay and MTT cell viability assay followed standard procedures and are detailed in the Supplementary Online Data.

ESI–IMS–MS data acquisition

All reagents and globular proteins were purchased from Sigma–Aldrich. All spectra were collected using a Synapt G2 HDMS instrument (Waters) by use of gold-coated home-made borosilicate nano-capillaries in positive-ion mode. Instrumental settings for data acquisition were: capillary voltage of 1.70–1.90 kV, cone voltage of 60 V, source temperature of 60 °C, trap collision energy of 4.0 V, transfer collision energy of 10 V, trap bias of 45, and backing pressure of 3.0–3.1 mbar (1 bar = 100 kPa). IMS separations were performed at T-wave velocities of

Trap: 311, IMS: 800 and Transfer: 200 m/s and T-wave amplitudes of 4–15 V using 3.6 mbar pressure of nitrogen gas maintained by a 90 ml/min gas flow. Mass calibration was carried out by an infusion of CsI cluster ions and the drift time cross-section function was calibrated as described previously [27,31]. Drift times were corrected for both mass-dependent and -independent TOF [27].

Molecular modelling

In silico Ω were calculated utilizing a modified version of the projection approximation script developed by the Ashcroft group [31,32]; the modified source code is available from https://github.com/tumbling-cross-section. Modifications to the original script included a change in the sweep patterns to a used a Fibonacci 'Pinecone' grid instead of the latitude–longitude scan [33] and the ability to use atomic radii of any value. *In silico* models were then created assuming the monomeric α-syn subunit was spherical with a radius of 19.9 Å (1 Å = 0.1 nm) which is comparable to the most compact observed form of the monomer measured here. Oligomers were modelled by allowing a 4 or 8 Å overlap between different subunits, giving a centre-to-centre distance of 36 or 32 Å which is comparable to the most compact forms of the dimer measured here. Models were then constructed by placing atoms 36 Å apart either in a sequential linear arrangement or by placing the centre of the spheres at the points of regular polygons in which the sides were 36 or 32 Å in length. The radius of the carbon atoms was set to 19.9 Å within the atomic radii library used by the projection approximation script. Supplementary Figure S1 shows an example of a hexagonal ring arrangement and associated PDB file.

RESULTS

In vitro, α-syn oligomers with distinct biophysical properties are associated with alternative mechanisms of neurotoxic activity, and protocols have been described for their production [6,29]. The gain-of-function is dependent on the method of oligomer preparation and falls into two main types: those with pore-forming capabilities which are able to induce Ca^{2+} influx resulting in cell death and those with seeding capabilities that are able to induce intracellular aggregation in a prion-like manner. Predominantly, these protocols use sodium phosphate or Tris as the buffer and these are both incompatible with MS; hence, the present study replaced the buffer with ammonium acetate which is MS-compatible. Oligomer formation was induced in ammonium acetate buffer following protocol 1 and the resulting oligomers were characterized by ESI–IMS–MS. The biochemical behaviour of the oligomers produced in ammonium acetate was then determined through comparisons with oligomers produced in sodium phosphate that have either pore-forming or intracellular-seeding abilities.

Native mass spectrometry to study molecular organization

ESI–IMS–MS allows the subunit size and gross morphology of protein complexes to be determined through the acquisition of Ω. These experimental results can then be compared with model structures to decipher the mechanism of assembly. Optimal instrumental settings were established and spectra of a range of globular proteins were acquired (Supplementary Table S1) [31,34]. Each of the spectra of the globular proteins displayed a narrow charge state distribution (CSD) indicative of a folded protein. Increasing the activation energies also resulted in increased Ω as the protein unfolded (results not
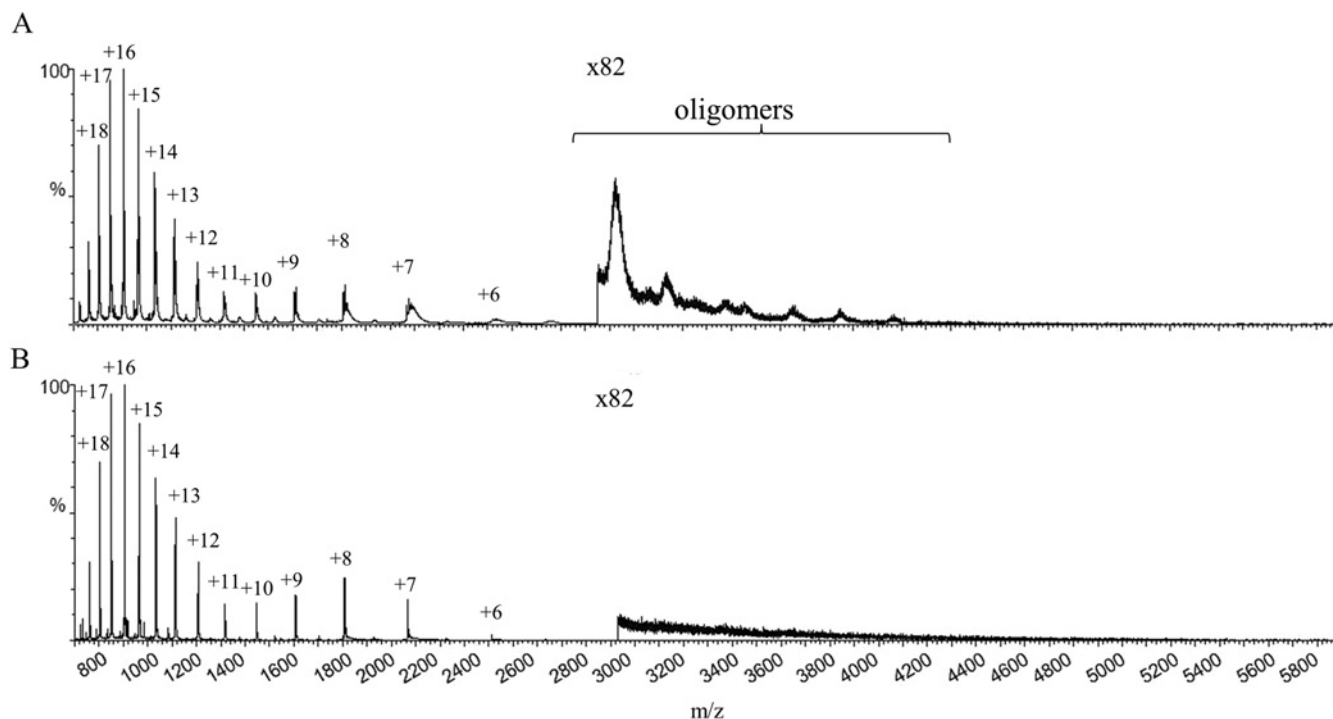
Figure 1 Comparison of ESI–MS spectra of 7 μM α-syn acquired in 50 mM ammonium acetate and 20% ethanol, pH 7.0

(**A**) Oligomers observed post-assembly and (**B**) monomeric α-syn in 50 mM ammonium acetate (pH 7.0) acquired immediately upon the addition of 20% ethanol showing the lack of any pre-existing oligomeric species. The x-axis represents m/z values, the y-axis is relative abundance (%). The region >2900 m/z was enlarged by 82-fold to visualize any of the lower-abundance oligomeric series.

shown), demonstrating that the proteins retain a native like conformation within our experiments. The monomeric form of α-syn is considered a natively disordered protein as it displays considerable conformational heterogeneity [35,36]. Analysis of WT α-syn before the addition of cofactors and ethanol revealed a primarily extended population (charge state ions $+8$ to $+18$) and a sub-population of a more compact conformational series (charge state ions $+6$ to $+8$) with multiple overlapping features consistent with previous data [34,37] (Figure 1). Critically, oligomeric forms were not detected immediately upon solvation and the addition of 20% ethanol, indicating that oligomers assemble as a result of the preparation protocols and are not induced by the act of spectral acquisition.

ESI–IMS–MS data were acquired to probe the structural properties of the α-syn oligomers assembled in ammonium acetate. Compactness and subunit arrangement of the oligomers were addressed through calculation of Ω for each charge state observed following established procedures [27,31]. Each oligomeric state was assigned based on multiples of the theoretical mass of the unmodified monomer. The mass spectrum and Driftscope plot of the α-syn oligomers revealed a range of oligomers from dimers to hexamers alongside both extended and compact populations of monomeric protein (Figures 1A and 2A). The presence of monomers to hexamers indicated that oligomer assembly progresses in an isotropic manner, recruiting one monomer at a time as oligomer size increased. To determine the gross morphological features of the oligomers, Ω were obtained for each of the charge state ions and compared with Ω of the globular protein structures (Supplementary Table S1). Figure 2B shows the mean Ω with the spread of the observed data for oligomers. The measured Ω of the globular standards was then used to back-calculate theoretical Ω assuming a spherical structure for a protein of a given mass (Figure 2B, black line).

The mean Ω of α-syn dimer was greater than that of porcine elastase and carbonic anhydrase (29 090 Da). The Ω of α-syn trimer was larger than the alcohol dehydrogenase (ADH) monomer (39 804 Da), whereas the α-syn pentamer Ω (72 300 Da) was greater than the Ω of the albumin monomer (66 463 Da). These results indicate that oligomers have a greater Ω than globular proteins of a comparable mass. In order to better illustrate the spread of Ω resulting from each oligomeric state, the observed Ω resulting from each charge state ion were plotted as a function of subunit sizes (Figure 3). Proteins that are unfolded are known to display a characteristic broad CSD, whereas folded globular proteins display a narrow CSD with a predicable mean charge [38]. The spread of dimers was quite remarkable in that the recorded range of Ω was 2407–4013 Å^2 with a CSD from $+9$ to $+16$ indicating a population of highly expanded to collapsed conformations. As the oligomer size increased, the range of experimental Ω measured decreased with the trimers spanning Ω of 3365–4454 Å^2, the tetramers spanning Ω of 4279–4695 Å^2, the pentamers spanning Ω of 4657–5015 Å^2 and the hexamers spanning Ω of 5414–5605 Å^2. The increase in oligomer size also resulted in narrower CSD; for example, the tetramers had a CSD of $+16$ to $+18$, the pentamers displayed charge state ions of $+17$ to $+20$, and hexamers obtained $+18$ to $+21$ charges. The measured Ω and CSD revealed that an increase in oligomer size resulted in increasingly compact oligomeric states with the pentamer and hexamer displaying a narrow CSD indicative of folded proteins [39]. The narrow CSD and relatively small Ω demonstrated that the higher-order oligomers obtain a compact conformation as they assemble as opposed to the structurally diverse and expanded states of the lower-order oligomers. The mean experimentally measured Ω of the α-syn oligomers were greater than that of predicted globular proteins, suggesting that they occupy more volume than the globular standards. The
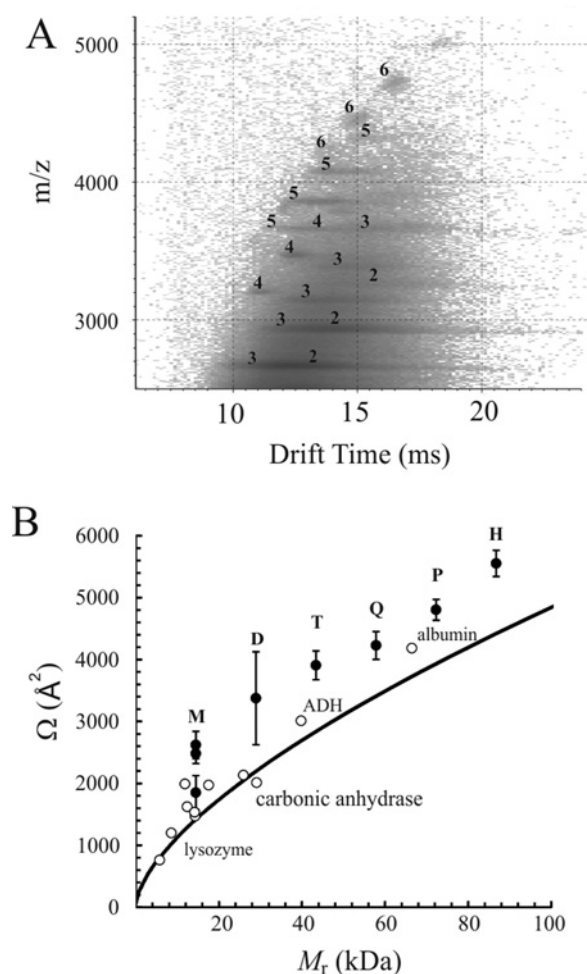
Figure 2   Driftscope plot of MS compatible oligomers with a comparison of Ω as a function molecular mass

(**A**) Driftscope plots and m/z spectra of α-syn oligomers. α-syn peaks were extracted from the Driftscope plots and the region >2900 m/z was enlarged to visualize the lower-abundance higher-order oligomeric series. Oligomers fell into the populations of dimers (2), trimers (3), tetramers (4), pentamers (5) and hexamers (6). (**B**) Comparison of Ω of α-syn oligomers (black circles) with that of globular protein standards (white circles) under native conditions. All measurements were carried out in triplicate and plotted as the mean Ω over all charge states against molecular mass (M_r). Error bars show the spread in Ω for monomeric (M), dimeric (D), trimeric (T), tetrameric (Q), pentameric (P) and hexameric (H) species; for details see Supplementary Table S1. The spread in Ω for the known globular standards can also be found in Supplementary Table S1. (black line). Theoretical Ω were calculated for a range molecular masses assuming a perfect sphere of density 0.37 Da/Å^3.

lower-order oligomers, indicated by their broad CSD, appear to be structurally diverse. However, the higher-order oligomers display a more compact structure indicated by the narrow CSD.

Modelling the topology of the oligomers

Computational approaches in conjunction with ESI–IMS–MS provide additional information when determining the potential geometries and structural features of multi-subunit systems [27,28]. To ascertain the topology of the oligomers, Ω were compared with theoretically derived Ω for a range of oligomeric conformations using a projection approximation algorithm [31]. This modelling approach assumes that the monomeric subunits of the higher-order oligomers are composed of fully folded sphere units with a 19.9 Å radius. This assumption is based on the narrow
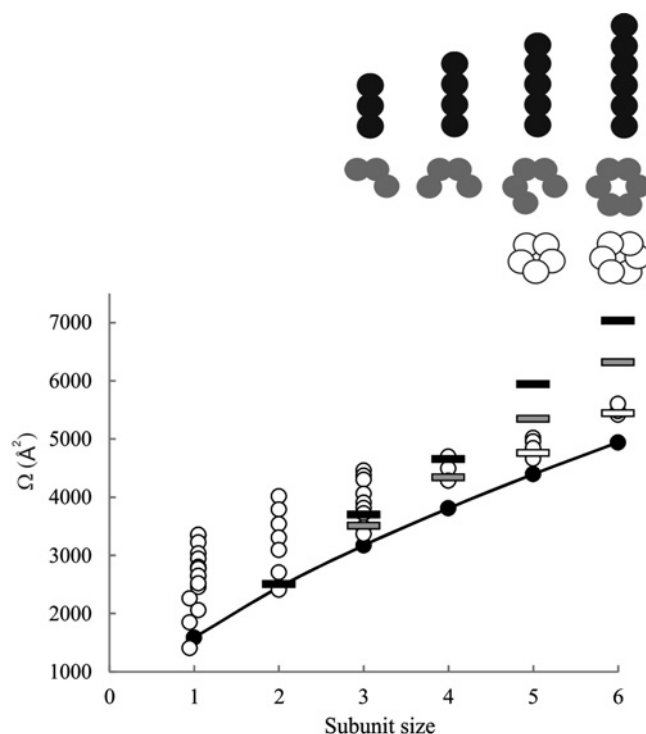

Figure 3   Ω of α-syn oligomers as a function of subunit size alongside model structures

Ω of each charge state ion are plotted according to oligomer size (white circles). The x-axis is subunit size and the y-axis shows Ω in Å^2. Expected Ω of model spherical structures with the same mass as the oligomers based on the globular protein standards are shown as black circles. Models were constructed by arranging subunits as spheres with a radii of 19.9 Å whose Ω is comparable to the most compact state of the monomer. Subunits were arranged either linearly (black lines), as ring and open ring arrangements with a centre-to-centre spacing of 36 Å (grey lines) or as a compact closed ring arrangement with a centre-to-centre spacing of 32 Å (white lines). A schematic representation of each of the models is shown above using the same colouring system.

CSD observed for the higher-order oligomers and each individual subunit being comparable to the most compact observed form of the monomer measured here (Figure 2). A 4 or 8 Å overlap between different subunits was allowed, giving a centre-to-centre distance of 36 or 32 Å which is comparable to the most compact forms of the dimer measured here. This modelling approach is similar to that used for the oligomers involved in Alzheimer's disease [40]. A range of conformations including linear structures, closed ring and open ring forms have been constructed to model the experimentally acquired Ω with centre-to-centre distance of 36 or 32 Å. The data were plotted alongside experimentally determined Ω for the oligomers of α-syn (Figure 3). Fully linear models and ring-like structures in which subunits are arranged with a spacing of 36 Å overestimated the observed Ω of the pentamers and hexamers. However, if the monomeric subunits were sequentially removed from this model *in silico* to create an open ring structure, then the most compact state of the tetramer could be modelled at 36 Å spacing. Partially collapsed models in which the oligomeric subunits are composed of a folded core made up of 100 amino acids with 40-amino-acid unstructured termini were also constructed (Supplementary Figure S2). These models are comparable with the more extended states of the tetramer but again overestimates the hexamer, supporting the notion that the higher-order oligomers are composed of compact subunits without the presence of unstructured termini. In order to model the experimental data compact closed rings with a
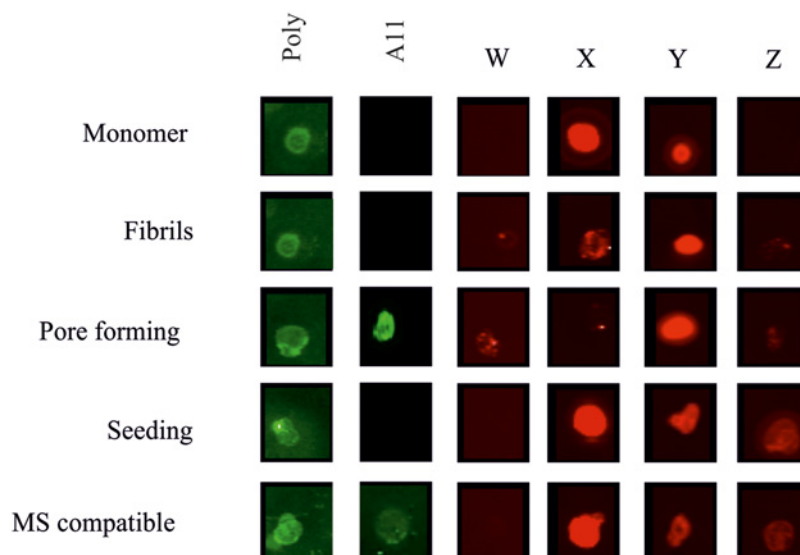
Figure 4   Epitope mapping profiles of α-syn monomer, fibrils and alternate oligomers

Epitope mapping studies of different oligomeric populations performed using mouse monoclonal antibodies, polyclonal anti-α-syn antibody (Poly) and anti-oligomer A11 antibody. Binding profile of monomer, fibril, pore-forming and seeding oligomers in ammonium acetate with polyclonal antibody, anti-α-syn antibody and monoclonal antibodies.

centre-to-centre distance of 32 Å were created. These models closely matched the observed experimental data for the hexamers and pentamer suggesting a compact ring-like arrangement for these oligomers. Fully spherical structures or closely packed arrangements underestimated the experimental data. Modelling the experimental data combined with the Ω and CSD analysis shows that as the oligomers assembled under MS-compatible conditions they become more compact structures, which are consistent with ring-like assemblies.

Oligomeric species show distinct epitopes by dot blotting

Dot blotting procedures are a standard method to determine the availability of antigenic conformational epitopes on the surface of oligomeric, protofibrillar or fibrillar species [41–44]. The α-syn oligomers were subjected to dot blotting with a rabbit polyclonal antibody (Poly) raised against full-length α-syn (Figure 4). All the samples bound to the Poly antibody except the BSA control, showing both specificity of the antibody and that all the oligomer samples contained α-syn protein (Figure 4). Oligomers were also probed with the conformation-dependent anti-oligomeric A11 antibody, which identifies oligomers linked to the Ca²⁺ influx toxic gain-of-function [45]. The oligomers prepared by protocol 1 (i.e., in sodium phosphate buffer) gave a strong fluorescent signal when probed with A11 (Figure 4). However, the oligomers produced in ammonium acetate (MS compatible) by this same protocol were only weakly reactive with A11, indicating that alternative structures may be present and/or there is a reduced yield. The monomer, fibrils and intracellular seeding oligomers were all unreactive to A11. In addition, a panel of mouse monoclonal antibodies denoted W, X, Y and Z (see the Supplementary Materials and methods section) directed against different epitopes of the three main domains (N-terminus, central region and C-terminus) of α-syn were used. Antibody W (N-terminal region) only detected the pore-forming oligomers prepared by protocol 1 in sodium phosphate buffer and none of the other forms. Monoclonal antibody X (mid-region) reacted with all the oligomers except the pore-forming oligomers, indicating that the epitope is buried and unavailable to bind. Monoclonal

antibody Y (C-terminal region) detected all oligomeric species, indicating that this region is exposed and accessible on all species. However, monoclonal antibody Z (C-terminal region) which overlaps with monoclonal with Y only showed reactivity with the seeding-type oligomers and the MS-compatible oligomers. This demonstrates that monoclonal antibodies Y and Z span a conformational hotspot in α-syn that is altered between the oligomeric forms. These results yielded a characteristic pattern for each oligomer type prepared in sodium phosphate buffers. MS-compatible oligomers assembled using ammonium acetate as a buffer displayed an epitope-binding pattern consistent with an intracellular seeding type (Figure 4).

Ca²⁺ influx and neurotoxicity

The dot blotting results predicted that the pore-forming oligomers produced by protocol 1 in sodium phosphate buffer would have Ca²⁺ channel-like behaviour due to their ability to bind the A11 antibody and the MS-compatible oligomers would be largely inactive in this assay. To test this hypothesis, the ability of each oligomeric type to induce Ca²⁺ influx was measured. SH-SY5Y neuroblastoma cells were cultured and loaded with a FLIPR Calcium 6-QF Ca²⁺ sensitive dye before treatment with the different oligomeric species [6]. As predicted, the pore-forming oligomers caused a rise in intracellular Ca²⁺ levels comparable to that caused by positive control ionomycin (Figure 5). None of the other oligomer types or controls (monomer and α-lactalbumin) had a comparable effect on intracellular Ca²⁺ levels. MTT viability assays performed at the same time point showed no significant loss in cell viability, indicating that Ca²⁺ influx was not a secondary effect of cell death (Supplementary Figure S3). After 48 h of treatment, only the pore-forming oligomers reduced the viability of the human neuroblastoma cells to statistically significant levels (Figure 6). These findings are in agreement with Danzer et al. [6], who showed that this oligomer type activated caspase-3 leading to apoptotic cell death. MS-compatible oligomers displayed a reduction in cell viability in accordance with the weak A11 reactivity (Figure 6).
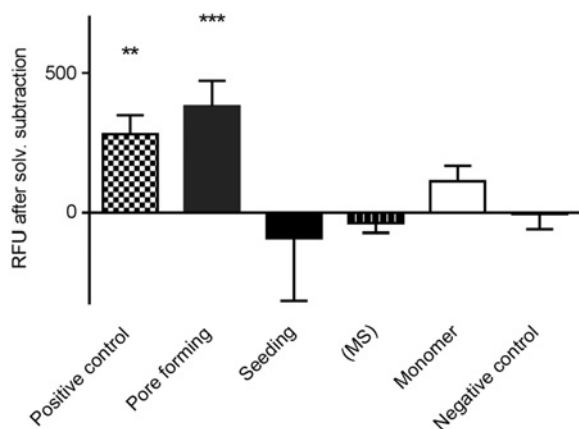
Figure 5 Ca²⁺ influx induced by the addition A11 positive oligomers

Ca^{2+} influx of SH-SY5Y human neuroblastoma cells performed at 1.0×10^5 cells/well seeding density. Appropriate solvents were subtracted and means have been plotted $\pm$S.E.M., $n = 3$, **$P < 0.001$ and ***$P < 0.0001$.
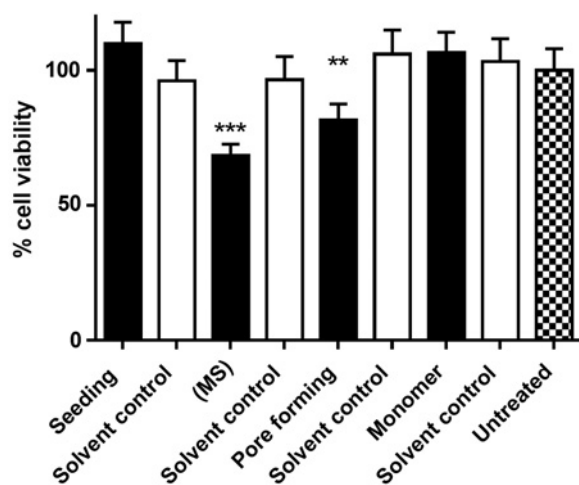

Figure 6 SH-SY5Y cell viability in the presence of α-syn monomer, fibrils and alternate oligomers

MTT cell viability assay of SH-SY5Y human neuroblastoma cells performed at 1.0×10^5 cells/well seeding density after 48 h of incubation with oligomers originating from protocol 1 or protocol 2 and MS-compatible oligomers alongside respective controls at 10 % (v/v). Means are plotted $\pm$S.E.M., values have been normalized to untreated cells (100 %). **$P < 0.001$, ***$P < 0.0001$.

Intracellular aggregation properties

Certain forms of α-syn located in the extracellular environment can be internalized and induce endogeneous α-syn to self-aggregate [6,18,46–49]. This may represent a mechanism for the spread of aggregated α-syn in the PD brain. To test the propensity of our oligomers to induce intracellular aggregation of α-syn, SH-SY5Y cells overexpressing A53T α-syn were exposed to each oligomer preparation as well as to the monomer and solvent controls (Figure 7). Treatment with the intracellular seeding oligomers produced by protocol 2 in sodium phosphate buffer caused a marked reduction in the homogeneous cytoplasmic staining of α-syn and resulted in an increase in punctate aggregates in the cytosol, consistent with Danzer et al. [29] (Figure 7B). In contrast, the A11-reactive pore-forming oligomers did not show any altered cytoplasmic staining, indicating that this form of oligomer lacked the ability to induce intracellular aggregation (Figure 7A).

MS-compatible oligomers had an enhanced ability to induce intracellular aggregation (Figure 7D). This correlated with their dot blotting profile which matched the intercellular seeding oligomers. Exposure to monomeric α-syn and the solvent controls did not result in aggregation (Figures 7C and 7F). The SH-SY5Y cells incubated with the MS-compatible oligomers for 20 min did not show any intracellular aggregation (Figure 7E). This demonstrated that formation of the punctate intracellular aggregates in Figures 7B and 7D was time-dependent and the observed punctuate aggregates were not an artefact brought about by pre-formed oligomers binding to the outside of the cell.

DISCUSSION

The properties of *in vitro* generated α-syn oligomers, with disease-relevant toxicity and aggregation properties, are dependent on the manner of preparation, resulting in either pore-forming or seeding types [6]. To understand the structure–function relationships of the α-syn oligomers, we modified the preparation protocols (by varying the buffer conditions) to allow them to be characterized by ESI–IMS–MS. In order to have a point of comparison for the oligomers produced under MS-compatible conditions, positive-control oligomers for both seeding and pore-forming oligomers were produced using previously described protocols. Seeding-type oligomers were non-toxic but able to induce intracellular aggregation, whereas the pore-forming oligomers were reactive to the anti-oligomer antibody A11 and brought about Ca^{2+} influx. In the present study, we have demonstrated that these positive-control oligomers have distinct differences in their surface-accessible epitopes with the MS-compatible oligomers produced in ammonium acetate matching the seeding-type oligomers produced in sodium phosphate. This similarity to the seeding-type oligomer was supported by the MS-compatible oligomers also being able to promoting intracellular seeding in cell culture. Only the pore-forming positive-control oligomers produced in sodium phosphate were able to induce toxicity and bind strongly to the A11 antibody. Some A11 binding was observed with the MS-compatible oligomers which had the ability to induce toxicity. The lyophilization step in protocol 1 may be critical for the increased formation of the A11-reactive species. Since ammonium acetate is a volatile buffer it will be removed by lyophilization, whereas sodium phosphate will remain. Hence the final ionic strength of the buffer on solubilization in the MS-compatible protocol will be lower as the volatile buffer has been removed. This difference in ionic strength presumably pushes the protein along one of two potential aggregation pathways upon resolubilization. By changing the assembly buffer from sodium phosphate to ammonium acetate, oligomers capable of intracellular seeding were produced.

The structure and topology of these oligomeric species were characterized by ESI–IMS–MS and found to co-populate dimers to hexamers, in addition to the presence of monomeric conformations. The presence of monomers to hexamers within the samples indicates isotopic growth and subunit assembly by monomer addition. Other groups, using alternative methods, have observed oligomer distributions akin to those seen here. Single-molecule FRET analysis has detected a range of α-syn oligomeric species that undergo a conformational change, resulting in higher-order oligomers and an increased resistance to proteinase K digestion over time [10]. The initial subset of oligomers ranged from dimers to pentamers in size and was prepared at the same concentrations used here. Therefore, it is possible that the oligomers characterized here represent the same initial subset of oligomers prior to their reorganization.
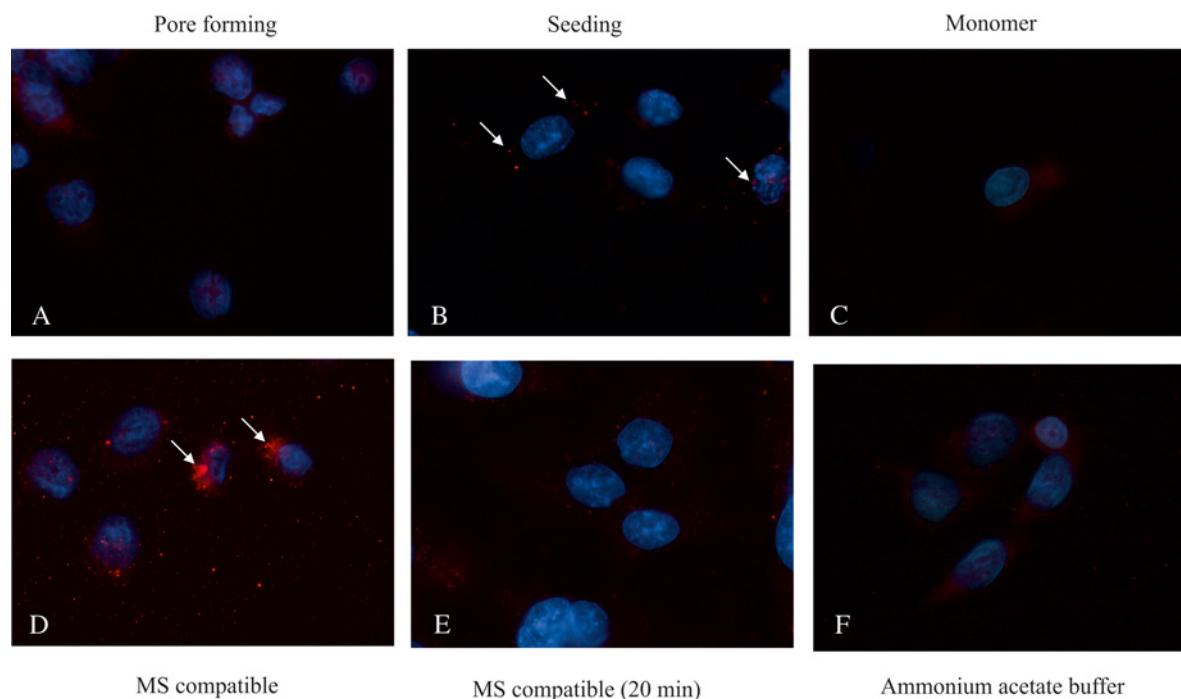
Figure 7   SH-SY5Y cells overexpressing the A53T α-syn variant were treated with 10 % (v/v) pre-formed oligomers, monomers or solvent for 8 h or 20 min

Immunofluorescent staining was performed with the A11 antibody (red staining) after treatment with 10 % (v/v) α-syn oligomers or matched solvent controls and was detected by Alexa Fluor® 495-conjugated goat anti-mouse antibody. DAPI staining appears blue; 100× magnification. The arrows indicate cells with punctate formation as a result of intracellular aggregation. Cells were treated with (**A**) pore-forming oligomers, (**B**) seeding-type oligomers, (**C**) α-syn monomer, (**D**) MS-compatible oligomers, (**E**) MS-compatible oligomers after a short incubation of 20 min and (**F**) ammonium acetate buffer vehicle control.

In vivo, oligomers characterized recently by number and brightness analysis in live SH-SH5Y cells also show a similar size range encompassing maximum 6 ± 4-mers, similar to our observations [50]. α-Syn is known to co-populate a range of conformational states as observed by ESI–IMS–MS. Our previous ESI–IMS–MS analysis of wild-type α-syn revealed a primarily extended population ($\sim 2482 \pm 159$ Å) and a subpopulation of two compact conformational series ($\sim 1851 \pm 276$ Å) with multiple overlapping features and a less observable dimeric species under native conditions [37] in accordance with previously published research [34]. The Barran group recently reported that α-syn displays a broad CSD ranging from $+5$ to $+21$ with a Ω of approximately 1600 Å. Chemical cross-linking with IMS–MS measurements revealed three main conformational families, a compact (~ 1200 Å), an extended (~ 1500 Å) and an unfolded (~ 2530 Å) state that are similar to monomeric conformers present in solution [51]. The existence of three distinct conformational states is in agreement with our observations; the inconsistencies between our Ω and those reported by this group may arise from experimental conditions including type of instrumentation, protein concentration and buffer conditions. Lower-order oligomers, in particular the dimers described in [51], had resulted from an alternative preparation protocol yet they were in agreement with our results reflecting conformationally dynamic entities. Przybylski and co-workers [52] have also undertaken characterization of α-syn oligomers by gel electrophoresis, N-terminal Edman sequencing and ion mobility measurements. Full-length monomeric and dimeric α-syn, proteolytic and truncated sequence fragments were identified in their investigations [52]. No higher-order oligomers were reported despite the use of similar preparation protocols to those discussed here. This may be due to the use of a desalting column operated at a gradient of 10–90 %

acetonitrile prior to IMS instrumentation which may disassemble the oligomers [52]. To determine the structural organization of the oligomers observed here Ω were calculated and revealed that as the subunit size increases, the oligomers become increasingly more compact. Lower-order oligomers (dimers and trimers) are structurally diverse and populate a broad range of Ω. Oligomers of the pentameric and hexameric series had very narrow CSD and little spread in their Ω, as compared with the lower-order oligomers and adopted structures that are consistent with a compact ring-like assembly that could not be fitted as linear, partially folded or spherical structures. This potentially compact ring model would explain why higher-order oligomers ($n > 6$) are not observed in the spectra as the further addition of monomers would require the ring-like structure to be broken and a conformational change to occur. The compact nature of the oligomers would protect them from degradation by proteases, allowing them to move from cell to cell and transmit pathology. Similar oligomeric conformations have been documented in the case of Aβ_{42} (where Aβ is amyloid β-peptide) oligomers, with dimers, tetramers, hexamers and dodecamers being observed and correlated with toxicity, but no odd number oligomers were detected. The higher-order oligomers obtained a ring-like structure very similar to that observed in our study [40,53] and ring assemblies have been observed by other methods such as AFM [54]. The structural collapse and assembly of α-syn seen on aggregation also has precedents. β_2-Microglobulin self-aggregation proceeds by monomeric addition at pH 2.5 where the initially highly expanded monomeric states collapse upon assembly to higher-order oligomers. However, in that system, the monomers to tetramers are more extended with Ω consistent with elongated structures and do not display the same toxic behaviour as Aβ_{42} and α-syn oligomers [55]. The energetics and complexity

governing the early stages of α-syn oligomerization has been illustrated by molecular modelling studies using a projection approximation algorithm which showed that each aggregated form of dimers, trimers and tetramers could have a number of different morphologies [56] akin to the dispersed Ω observed here. Although we cannot rule out higher-order species being present, they were not observed by ESI–IMS–MS as was the case for the single-molecule FRET experiments [10]. Future investigations should focus on an in-depth analysis of the kinetics and stability of these α-syn oligomers and how that correlates to toxicity and propagation.

From the results we have gathered here, we speculate that compact higher-order ring-like oligomers are associated with intracellular seeding. This proposal provides a guide for directing efforts towards the isolation of the toxic forms α-syn *in vivo*. As such, it would be highly desirable to obtain more comprehensive information about α-syn oligomers that have been detected in the cerebrospinal fluid and sera of PD patients [13–16] through the epitope mapping used here. The challenge will remain to isolate oligomers from clinical specimens of PD patients or other biological systems under near-native conditions [57,58] and elucidate how the oligomers produced *in vivo* compare with those observed here.

AUTHOR CONTRIBUTION

ACKNOWLEDGEMENTS

FUNDING

REFERENCES

1 Lashuel, H. A., Overk, C. R., Oueslati, A. and Masliah, E. (2013) The many faces of alpha-synuclein: from structure and toxicity to therapeutic target. Nat. Rev. Neurosci. **14**, 38–48 CrossRef PubMed

2 Forno, L. S. (1996) Neuropathology of Parkinson's disease. J. Neuropathol. Exp. Neurol. **55**, 259–272 CrossRef PubMed

3 Fujioka, S., Ogaki, K., Tacik, P. M., Uitti, R. J., Ross, O. A. and Wszolek, Z. K. (2014) Update on novel familial forms of Parkinson's disease and multiple system atrophy. Parkinsonism Relat. Disord. **20** (Suppl. 1), S29–S34 CrossRef PubMed

4 Brown, D. R. (2010) Oligomeric alpha-synuclein and its role in neuronal death. IUBMB Life **62**, 334–339 PubMed

5 Kalia, L. V., Kalia, S. K., McLean, P. J., Lozano, A. M. and Lang, A. E. (2013) α-Synuclein oligomers and clinical implications for Parkinson disease. Ann. Neurol. **73**, 155–169 CrossRef PubMed

6 Danzer, K. M., Haasen, D., Karow, A. R., Moussaud, S., Habeck, M., Giese, A., Kretzschmar, H., Hengerer, B. and Kostka, M. (2007) Different species of alpha-synuclein oligomers induce calcium influx and seeding. J. Neurosci. **27**, 9220–9232 CrossRef PubMed

7 van Rooijen, B. D., Claessens, M. M. and Subramaniam, V. (2010) Membrane permeabilization by oligomeric alpha-synuclein: in search of the mechanism. PLoS One **5**, e14292 CrossRef PubMed

8 Giehm, L., Svergun, D. I., Otzen, D. E. and Vestergaard, B. (2011) Low-resolution structure of a vesicle disrupting & alpha;-synuclein oligomer that accumulates during fibrillation. Proc. Natl. Acad. Sci. U.S.A. **108**, 3246–3251 CrossRef PubMed

9 Nasstrom, T., Fagerqvist, T., Barbu, M., Karlsson, M., Nikolajeff, F., Kasrayan, A., Ekberg, M., Lannfelt, L., Ingelsson, M. and Bergstrom, J. (2011) The lipid peroxidation products 4-oxo-2-nonenal and 4-hydroxy-2-nonenal promote the formation of alpha-synuclein oligomers with distinct biochemical, morphological, and functional properties. Free Radic. Biol. Med. **50**, 428–437 CrossRef PubMed

10 Cremades, N., Cohen, S. I., Deas, E., Abramov, A. Y., Chen, A. Y., Orte, A., Sandal, M., Clarke, R. W., Dunne, P., Aprile, F. A. et al. (2012) Direct observation of the interconversion of normal and toxic forms of alpha-synuclein. Cell **149**, 1048–1059 CrossRef PubMed

11 Singh, P. K., Kotia, V., Ghosh, D., Mohite, G. M., Kumar, A. and Maji, S. K. (2013) Curcumin modulates alpha-synuclein aggregation and toxicity. ACS Chem. Neurosci. **4**, 393–407 CrossRef PubMed

12 Marques, O. and Outeiro, T. F. (2012) Alpha-synuclein: from secretion to dysfunction and death. Cell Death Dis. **3**, e350 CrossRef PubMed

13 El-Agnaf, O. M., Salem, S. A., Paleologou, K. E., Curran, M. D., Gibson, M. J., Court, J. A., Schlossmacher, M. G. and Allsop, D. (2006) Detection of oligomeric forms of alpha-synuclein protein in human plasma as a potential biomarker for Parkinson's disease. FASEB J. **20**, 419–425 CrossRef PubMed

14 Tokuda, T., Qureshi, M. M., Ardah, M. T., Varghese, S., Shehab, S. A., Kasai, T., Ishigami, N., Tamaoka, A., Nakagawa, M. and El-Agnaf, O. M. (2010) Detection of elevated levels of alpha-synuclein oligomers in CSF from patients with Parkinson disease. Neurology **75**, 1766–1772 CrossRef PubMed

15 Foulds, P. G., Yokota, O., Thurston, A., Davidson, Y., Ahmed, Z., Holton, J., Thompson, J. C., Akiyama, H., Arai, T., Hasegawa, M. et al. (2012) Post mortem cerebrospinal fluid alpha-synuclein levels are raised in multiple system atrophy and distinguish this from the other alpha-synucleinopathies, Parkinson's disease and Dementia with Lewy bodies. Neurobiol. Dis. **45**, 188–195 CrossRef PubMed

16 Toledo, J. B., Korff, A., Shaw, L. M., Trojanowski, J. Q. and Zhang, J. (2013) CSF alpha-synuclein improves diagnostic and prognostic performance of CSF tau and Abeta in Alzheimer's disease. Acta Neuropathol. **126**, 683–687 CrossRef PubMed

17 Prusiner, S. B. (2012) Cell biology. A unifying role for prions in neurodegenerative diseases. Science **336**, 1511–1513 CrossRef PubMed

18 Aulic, S., Le, T. T., Moda, F., Abounit, S., Corvaglia, S., Casalis, L., Gustincich, S., Zurzolo, C., Tagliavini, F. and Legname, G. (2014) Defined alpha-synuclein prion-like molecular assemblies spreading in cell culture. BMC Neurosci. **15**, 69 CrossRef

19 Sacino, A. N., Thomas, M. A., Ceballos-Diaz, C., Cruz, P. E., Rosario, A. M., Lewis, J., Giasson, B. I. and Golde, T. E. (2013) Conformational templating of alpha-synuclein aggregates in neuronal-glial cultures. Mol. Neurodegener. **8**, 17 PubMed

20 Chauhan, A. and Jeans, A. F. (2015) Is Parkinson's disease truly a prion-like disorder? An appraisal of current evidence. Neurol. Res. Int. **2015**, 345285 CrossRef PubMed

21 Oueslati, A., Ximerakis, M. and Vekrellis, K. (2014) Protein transmission, seeding and degradation: key steps for alpha-synuclein prion-like propagation. Exp. Neurobiol. **23**, 324–336 CrossRef PubMed

22 Beyer, K. and Ariza, A. (2013) Alpha-synuclein posttranslational modification and alternative splicing as a trigger for neurodegeneration. Mol. Neurobiol. **47**, 509–524 CrossRef PubMed

23 Liu, Y., Carver, J. A., Calabrese, A. N. and Pukala, T. L. (2014) Gallic acid interacts with alpha-synuclein to prevent the structural collapse necessary for its aggregation. Biochim. Biophys. Acta **1844**, 1481–1485 CrossRef PubMed

24 Santner, A. and Uversky, V. N. (2010) Metalloproteomics and metal toxicology of alpha-synuclein. Metallomics **2**, 378–392 CrossRef PubMed

25 Lucas, H. R. and Lee, J. C. (2011) Copper(II) enhances membrane-bound alpha-synuclein helix formation. Metallomics **3**, 280–283 CrossRef PubMed

26 Ashcroft, A. E. (2010) Mass spectrometry and the amyloid problem–how far can we go in the gas phase? J. Am. Soc. Mass Spectrom. **21**, 1087–1096 CrossRef PubMed

27 Ruotolo, B. T., Benesch, J. L., Sandercock, A. M., Hyung, S. J. and Robinson, C. V. (2008) Ion mobility-mass spectrometry analysis of large protein complexes. Nat. Protoc. **3**, 1139–1152 CrossRef PubMed

28 Politis, A., Park, A. Y., Hyung, S. J., Barsky, D., Ruotolo, B. T. and Robinson, C. V. (2010) Integrating ion mobility mass spectrometry with molecular modelling to determine the architecture of multiprotein complexes. PLoS One **5**, e12080 CrossRef PubMed

29 Danzer, K. M., Krebs, S. K., Wolff, M., Birk, G. and Hengerer, B. (2009) Seeding induced by alpha-synuclein oligomers provides evidence for spreading of alpha-synuclein pathology. J. Neurochem. **111**, 192–203 CrossRef PubMed

30 Smith, D. P., Tew, D. J., Hill, A. F., Bottomley, S. P., Masters, C. L., Barnham, K. J. and Cappai, R. (2008) Formation of a high affinity lipid-binding intermediate during the early aggregation phase of alpha-synuclein. Biochemistry **47**, 1425–1434 CrossRef PubMed

31 Smith, D. P., Knapman, T. W., Campuzano, I., Malham, R. W., Berryman, J. T., Radford, S. E. and Ashcroft, A. E. (2009) Deciphering drift time measurements from travelling wave ion mobility spectrometry-mass spectrometry studies. Eur. J. Mass. Spectrom. (Chichester, Eng.) **15**, 113–130 CrossRef PubMed

32 Knapman, T. W., Berryman, J. T., Campuzano, I., Harris, S. A. and Ashcroft, A. E. (2010) Considerations in experimental and theoretical collision cross-section measurements of small molecules using travelling wave ion mobility spectrometry-mass spectrometry. Int. J. Mass. Spectrom. **298**, 17–23 CrossRef

33 Gonzales, A. (2010) Measurement of areas on a sphere using Fibonacci and latitude-longitude lattices. Math. Geosci. **42**, 49–64 CrossRef

34 Bernstein, S. L., Liu, D., Wyttenbach, T., Bowers, M. T., Lee, J. C., Gray, H. B. and Winkler, J. R. (2004) Alpha-synuclein: stable compact and extended monomeric structures and pH dependence of dimer formation. J. Am. Soc. Mass Spectrom. **15**, 1435–1443 CrossRef PubMed

35 Beveridge, R., Chappuis, Q., Macphee, C. and Barran, P. (2013) Mass spectrometry methods for intrinsically disordered proteins. Analyst **138**, 32–42 CrossRef PubMed

36 Beveridge, R., Covill, S., Pacholarz, K. J., Kalapothakis, J. M., MacPhee, C. E. and Barran, P. E. (2014) A mass-spectrometry-based framework to define the extent of disorder in proteins. Anal. Chem. **86**, 10979–10991 CrossRef PubMed

37 Illes-Toth, E., Dalton, C. F. and Smith, D. P. (2013) Binding of dopamine to alpha-synuclein is mediated by specific conformational states. J. Am. Soc. Mass Spectrom. **24**, 1346–1354 CrossRef PubMed

38 Heck, A. J. and Van Den Heuvel, R. H. (2004) Investigation of intact protein complexes by mass spectrometry. Mass Spectrom. Rev. **23**, 368–389 CrossRef PubMed

39 Kaltashov, I. A. and Mohimen, A. (2005) Estimates of protein surface areas in solution by electrospray ionization mass spectrometry. Anal. Chem. **77**, 5370–5379 CrossRef PubMed

40 Bernstein, S. L., Dupuis, N. F., Lazo, N. D., Wyttenbach, T., Condron, M. M., Bitan, G., Teplow, D. B., Shea, J. E., Ruotolo, B. T., Robinson, C. V. and Bowers, M. T. (2009) Amyloid-beta protein oligomerization and the importance of tetramers and dodecamers in the aetiology of Alzheimer's disease. Nat. Chem. **1**, 326–331 CrossRef PubMed

41 Kayed, R. and Glabe, C. G. (2006) Conformation-dependent anti-amyloid oligomer antibodies. Methods Enzymol. **413**, 326–344 CrossRef PubMed

42 Yanamandra, K., Gruden, M. A., Casaite, V., Meskys, R., Forsgren, L. and Morozova-Roche, L. A. (2011) alpha-synuclein reactive antibodies as diagnostic biomarkers in blood sera of Parkinson's disease patients. PLoS One **6**, e18513 CrossRef PubMed

43 Colla, E., Jensen, P. H., Pletnikova, O., Troncoso, J. C., Glabe, C. and Lee, M. K. (2012) Accumulation of toxic alpha-synuclein oligomer within endoplasmic reticulum occurs in alpha-synucleinopathy in vivo. J. Neurosci. **32**, 3301–3305 CrossRef PubMed

44 Guilliams, T., El-Turk, F., Buell, A. K., O'Day, E. M., Aprile, F. A., Esbjorner, E. K., Vendruscolo, M., Cremades, N., Pardon, E., Wyns, L. et al. (2013) Nanobodies raised against monomeric alpha-synuclein distinguish between fibrils at different maturation stages. J. Mol. Biol. **425**, 2397–2411 CrossRef PubMed

45 Kayed, R., Head, E., Thompson, J. L., McIntire, T. M., Milton, S. C., Cotman, C. W. and Glabe, C. G. (2003) Common structure of soluble amyloid oligomers implies common mechanism of pathogenesis. Science **300**, 486–489 CrossRef PubMed

46 Luk, K. C., Song, C., O'Brien, P., Stieber, A., Branch, J. R., Brunden, K. R., Trojanowski, J. Q. and Lee, V. M. (2009) Exogenous alpha-synuclein fibrils seed the formation of Lewy body-like intracellular inclusions in cultured cells. Proc. Natl. Acad. Sci. U.S.A. **106**, 20051–20056 CrossRef PubMed

47 Danzer, K. M., Kranich, L. R., Ruf, W. P., Cagsal-Getkin, O., Winslow, A. R., Zhu, L., Vanderburg, C. R. and McLean, P. J. (2012) Exosomal cell-to-cell transmission of alpha synuclein oligomers. Mol. Neurodegener. **7**, 42 CrossRef PubMed

48 Angot, E., Steiner, J. A., Lema Tome, C. M., Ekstrom, P., Mattsson, B., Bjorklund, A. and Brundin, P. (2012) Alpha-synuclein cell-to-cell transfer and seeding in grafted dopaminergic neurons in vivo. PLoS One **7**, e39465 CrossRef PubMed

49 Hansen, C., Angot, E., Bergstrom, A. L., Steiner, J. A., Pieri, L., Paul, G., Outeiro, T. F., Melki, R., Kallunki, P. et al. (2011) alpha-Synuclein propagates from mouse brain to grafted dopaminergic neurons and seeds aggregation in cultured human cells. J. Clin. Invest. **121**, 715–725 CrossRef PubMed

50 Plotegher, N., Gratton, E. and Bubacco, L. (2014) Number and Brightness analysis of alpha-synuclein oligomerization and the associated mitochondrial morphology alterations in live cells. Biochim. Biophys. Acta **1840**, 2014–2024 CrossRef PubMed

51 Phillips, A. S., Gomes, A. F., Kalapothakis, J. M., Gillam, J. E., Gasparavicius, J., Gozzo, F. C., Kunath, T., MacPhee, C. and Barran, P. E. (2015) Conformational dynamics of alpha-synuclein: insights from mass spectrometry. Analyst **140**, 3070–3081 PubMed

52 Vlad, K., Iurascu, M. I., Slamnoiu, S., Hengerer, B. and Przybylski, M. (2012) Characterisation of oligomerization-aggregation products of neurodegenerative target proteins by ion mobility mass spectrometry. Methods Mol. Biol. **896**, 399–412 CrossRef PubMed

53 Clemmer, D. E. and Valentine, S. J. (2009) Bioanalytical chemistry: protein oligomers frozen in time. Nat. Chem. **1**, 257–258 CrossRef PubMed

54 Quist, A., Doudevski, I., Lin, H., Azimova, R., Ng, D., Frangione, B., Kagan, B., Ghiso, J. and Lal, R. (2005) Amyloid ion channels: a common structural link for protein-misfolding disease. Proc. Natl. Acad. Sci. U.S.A. **102**, 10427–10432 CrossRef PubMed

55 Smith, D. P., Radford, S. E. and Ashcroft, A. E. (2010) Elongated oligomers in beta2-microglobulin amyloid assembly revealed by ion mobility spectrometry-mass spectrometry. Proc. Natl. Acad. Sci. U.S.A. **107**, 6794–6798 CrossRef PubMed

56 Gurry, T., Ullman, O., Fisher, C. K., Perovic, I., Pochapsky, T. and Stultz, C. M. (2013) The dynamic structure of alpha-synuclein multimers. J. Am. Chem. Soc. **135**, 3865–3872 CrossRef PubMed

57 Bartels, T., Choi, J. G. and Selkoe, D. J. (2011) alpha-Synuclein occurs physiologically as a helically folded tetramer that resists aggregation. Nature **477**, 107–110 CrossRef PubMed

58 Fauvet, B., Mbefo, M. K., Fares, M. B., Desobry, C., Michael, S., Ardah, M. T., Tsika, E., Coune, P., Prudent, M., Lion, N. et al. (2012) alpha-Synuclein in central nervous system and from erythrocytes, mammalian cells, and Escherichia coli exists predominantly as disordered monomer. J. Biol. Chem. **287**, 15345–15364 CrossRef PubMed

Structural characterisation of oligomeric alpha-synuclein with the ability to induce intracellular aggregation

Eva Illes-Toth*[‡], Mafalda Ribeiro Ramos*, Roberto Cappai[†], Caroline Dalton*, and David P Smith*

*. Biomedical Research Centre, Sheffield Hallam University, Howard Street, Sheffield, S1 1WB, UK

[†]. Department of Pathology, Bio21 Molecular Science and Biotechnology Institute, The University of Melbourne, Victoria 3010, Australia

[‡] current address, Washington University in St. Louis, Saint Louis, MO, USA

To whom correspondence should be addressed: Dr David Smith. Department of Biosciences, Sheffield Hallam University, Howard Street, Sheffield, S1 1WB, UK

E-mail: d.p.smith@shu.ac.uk Tel. +44 (0)114 2253044 Fax. +44 (0)114 2253066

Extended Materials and Methods

Preparation of α-Syn oligomers Monomeric α-syn was expressed in *E. coli* BL21(DE3) strain and purified as described before [1]. Protein concentration was measured by absorbance at 280 nm with extinction coefficient 5960 $M^{-1}cm^{-1}$ on a Jenway 6715 UV/Vis Spectrophotometer. All oligomers were prepared as described by Danzer *et al.* unless otherwise stated [2]. To make oligomers suitable for ESI-IMS-MS 50 mM sodium phosphate buffer was replaced with 50 mM ammonium acetate, pH 7.0 and relates to procedures that referred to oligomers prepared under mass spectrometry suitable conditions.

Pore forming oligomer protocol 1: Oligomers were prepared by dissolving the lyophilised monomeric α-syn protein in 50 mM sodium phosphate in deionised water or ammonium acetate, containing 20% ethanol to a final concentration of 7 μM. After 4 h of shaking, oligomers were freeze-dried and resuspended with one-half of starting volume in 50 mM starting buffer, pH 7.0, containing 10% ethanol. This was followed by shaking for 24 h (Thermomixer, Eppendorf, Germany) at 21^0C with open lids to evaporate residual ethanol. After 6 day incubation of oligomers with closed lids at 21^0C the oligomers were used for characterisation by a combination of techniques.

Seeding oligomer protocol 2: Oligomers were also prepared by dissolving the lyophilised monomeric protein in 50 mM sodium phosphate pH 7.0, containing 20% ethanol to a final concentration of 7 μM. After overnight incubation at 21^0C with continuous shaking (Thermomixer, Eppendorf, Germany), the oligomers were concentrated and separated from monomer using a MWCO 30 kDa filter (VivaSpin500 30,000 MWCO columns; Sartorius).

Epitope mapping procedure by dot blotting 1 μL of each oligomer, α-syn monomer or BSA was pipetted onto nitrocellulose membrane and air dried before the addition of 2% w/v BSA blocking solution in PBS pH 7.2 for 30 min. After blocking the primary antibody was added diluted in PBS-T containing 10% v/v BSA blocking solution. The commercially available antibody, A11 anti-amyloid oligomeric rabbit polyclonal antibody (epitope: n/a; oligomeric; Millipore) was used at dilution of 1:1000. The following anti- α-syn monoclonal antibodies were generated using the Walter and Eliza Hall Institute Monoclonal Antibody Facility, Australia.

W. 35/10 7D2 mouse monoclonal, epitope: MDVFMKGLSKAKC, 1:400 dilution

X. 31/09 4H4-14-27-12 mouse monoclonal, epitope: KKDQLGK, 1: 20,000 dilution

Y. syn 211 anti-α-syn mouse monoclonal antibody (Sigma), epitope: DNEAY, 1: 1,000 dilution

Z. 45/08 5G7-1 mouse monoclonal, epitope: EAYEMP, 1:30,000 dilution

An anti-α-syn rabbit polyclonal antibody (Poly) used at 1:50,000 dilution that was generated against full-length recombinant α-syn was generated using the Walter and Eliza Hall Institute Monoclonal Antibody Facility, Australia. It was included to confirm the presence of the α-syn.

All primary antibodies were incubated for 1 h at room temperature followed by three 10 min washes in PBS-T. For detection of antibodies raised in mouse, goat anti-mouse IR Dye^R 680 LT IgG (H+L) fluorescent secondary antibody (Odyssey) was utilised at 1:20, 000 dilution. For detection of epitopes recognised by the full anti α-syn rabbit polyclonal antibody and the A11 antibody, goat anti-rabbit IR Dye^R 800 CW IgG (H+L) fluorescent secondary antibody (Odyssey) was used at 1:15, 000 dilution.

Cell culture of SH-SY5Y cells and SH-SY5Y cells overexpressing A53T mutant of α-syn
SH-SY5Y human neuroblastoma cells were maintained and grown in complete Dulbecco's modified Eagle medium (CDMEM) consisting of 500 mL DMEM+ GlutaMAX^{TM} –II (Gibco), 50 mL fetal bovine serum (Biosera, heat inactivated, qualified), 5 mL Pen Strep (Penicillin Streptomycin, 5000 units/mL penicillin, 500 µg/mL streptomycin, Gibco) up to maximum 20 passages. The identity of the cell line was confirmed by a 16 loci Cell Line Authentication certificate. Transient transfection and then a stable transfection with the familial A53T mutant subcloned into the pcDNA3.1 vector was established using Lipofectamine transfection reagent according to the manufacturer's protocol. Stepwise dilution cloning was performed by picking individual transformed colonies cultured in CDEM with the addition of 200 µg/mL selective G418 antibiotics (Sigma, G8168-10 mL) and overexpression of the A53T mutant was confirmed by immunocytochemistry and Western blotting.

MTT cell viability assay SH-SY5Y human neuroblastoma cells were seeded in a 96-well plate at a density of 1×10^5 cells/well and cultured overnight. Next day the cells were treated with respective α-syn oligomers at 10% v/v (0.01 mg/mL referring to the monomer's concentration) and 7 µM monomer in the presence of appropriate solvent and positive controls and incubated for 4 h, and 48 h at 37 °C, 5% CO_2. Subsequently, 20 µL of 5 mg/mL MTT [3-(4,5-dimethylthiaziazol-2-yl)-2,5-diphenyl-2H-tetrazolium bromide] (Sigma) was added to each well and incubated for a further 4 h. The medium was then removed followed by the addition of 150 µL of DMSO to dissolve the purple formazan crystals. After 15 min agitation at room temperature, the color intensity was read at 570 nm and 650 nm on the Tecan Infinite 200M plate reader. The data was analyzed by the GraphPadPrism software to evaluate the statistical difference; values were expressed as mean ± SEM normalised to untreated cells (100% viability). One-way ANOVA followed by Bonferroni post-hoc test was used to establish whether significant differences existed among various treatment groups.

Ca^{2+} influx assay SH-SY5Y cell were cultured and seeded the day before the assay at 1×10^5 cells/well density in CDMEM in 96 well black/clear, tissue culture treated, flat bottom fluorescent imaging plates (BD Biosciences). FLIPR Calcium 6-QF Assay Kit (Molecular Devices, R8192) was used. The FLIPR Calcium 6-QF fluorophore was reconstituted in Krebs Ringer buffer (Sigma) supplemented with 1 mM $CaCl_2$ and 20 mM HEPES to 2X working strength and used to replace the medium of the SH-SY5Y cells seeded in CDMEM next day. The fluorophore loaded cells in modified Krebs Ringer buffer (50 µL/well) were incubated for 120 min at 37^0C at 5% CO_2 in dark conditions. The various oligomers were prepared to a 10% v/v final concentration (for oligomers 0.01 mg/mL referring to the monomer's concentration) and ionomycin (Sigma) positive control to a 5 µM final concentration in modified Krebs Ringer buffer and equal volumes of the various oligomers, vehicles and controls were injected directly onto the cells before measurement. The fluorescent intensity was measured at 485 nm and 535 nm on a Tecan Infinite 200M plate reader. At regular time intervals, the intensities were collected and 60 min after injection readings were stopped. After appropriate solvent subtraction values were analyzed by one-way ANOVA using Bonferroni multiple comparison test for selected pairs and expressed as mean± SEM. Data included here was plotted at the 60 min time point.

Immunocytochemistry SH-SY5Y cells overexpressing the familiar mutant A53T α-syn were maintained in CDMEM supplemented with 200 μL/mL G418 antibiotics. Cells were seeded in CDMEM in 8 well Lab-Tek II chamber slides (Nunc) at 0.5×10^5 cells/ mL seeding density and 600 μL cell suspension was added for each chamber and grown to ~70 % confluence. Treatment groups were added in the presence of appropriate vehicle controls at 10% v/v (0.01 mg/mL concentration referring to the monomer's concentration) for 8 h or 20 min treatment. Thereafter, the culture media was removed from the chambers and the cells were fixed with ice cold methanol for 15 min, followed by 3x three min wash with PBS-T and 5 min incubation with 0.5% v/v Triton–X100 (Sigma) in PBS to permeabilize cells. Then another 3x three min wash were carried out in PBS-T before blocking with 2% w/v BSA and the appropriate primary antibody (syn 211, mouse monoclonal antibody was added at a 1:1000 dilution for overnight incubation at 4^0C or for 1 h at room temperature. This was followed 3x three min wash with PBS-T. The secondary fluorescent antibody, Alexa Fluor$^®$ 594 conjugated goat anti-mouse antibody at a 1:1000 dilution (Molecular Probes, Invitrogen) was incubated for 1 h at room temperature. A 2x three min wash with PBS-T followed the secondary incubation step before adding 0.5 mg/mL 4'6-diamidine-2'-phenylindole dihydrochloride (DAPI) (Sigma) for counterstaining the nuclei. After DAPI staining one three minute washing step was performed, slides were further incubated in MQ water for 4 days. Mounting was carried out by using non-fluorescent immersion oil (Sigma 56822). Each chamber was covered by glass coverslips for visualisation by fluorescent microscopy on an Olympus BX60 microscope under oil immersion. To assess background fluorescence, primary antibody was omitted in a designated chamber and all other stages were the same as described above. Acquisition settings of Capture Pro6 software were on an Olympus BX60 microscope using a 100x oil immersion objective. Pseudo-colours were extracted and recombined after acquisition to obtain merged images.

ESI-IMS-MS instrumental settings and data acquisition All reagents and globular proteins were purchased from Sigma-Aldrich, UK. All spectra were collected using a Synapt G2 HDMS instrument (Waters, Manchester, UK) by use of gold coated home-made borosilicate nano-capillaries in positive mode. Instrumental settings were extensively optimised by varying the backing pressure, bias, cone and capillary voltages of the standards predominantly under native conditions. Optimised instrumental settings for data acquisition were: capillary voltage of 1.70-1.90 kV, cone voltage of 60 V, source temperature of 60^oC,

trap collision energy of 4.0 V, transfer collision energy of 10 V, trap bias 45, backing pressure of 3.0-3.1 mbar. IMS separations were performed at T-wave velocities of Trap:311, IMS:800 and Transfer:200 m/s and T-wave amplitudes of 4-15 V using 3.6 mbar pressure of nitrogen gas maintained by a 90 mL/ min gas flow. Native spectra were obtained by dissolving the protein in question to a 10-20 μM final concentration in aqueous solution of 50 mM ammonium acetate at pH 6.8 or pH 7.0. α-syn oligomers were prepared as above. For attaining denatured spectra, all calibrants and mass standards were prepared before injection at 10-20 μM and α-syn at 10 and 40 μM and dissolved in 50% acetonitrile, 10% formic acid and 40% ultrapure water (v/v/v). Calibration curve for Ωs was obtained based on of multiple charge states of cytochrome c from horse heart, myoglobin from equine heart and ubiquitin from bovine erythrocytes as described previously [3, 4]. Alcohol dehydrogenase (ADH) from yeast, α-lactalbumin from bovine milk, carbonic anhydrase from bovine erythrocytes, bovine albumin, bovine insulin, lysozyme from chicken egg and porcine elastase from porcine pancreas were purchased from Sigma, UK and ESI-IMS-MS data for each protein was obtained in the same manner. Mass calibration was carried out by an infusion of CsI cluster ions, and arrival time distributions were determined by using the Mass Lynx v4.1 software (Waters, Manchester, UK).

ESI-IMS-MS Modelling Computer-based cross-sectional area estimations were calculated from *in silico* models utilizing a Windows-based, in-house projection approximation algorithm described previously [5, 6]. Modifications to the original script included a change in the sweep patterns to a used a Fibonacci "Pinecone" grid instead of the Latitude-Longitude scan [7] and the ability to use atomic radii of any value. *In silico* models were created assuming the monomeric α-syn subunit was spherical with a radius of 19.9 Å which is comparable to the most compact observed form of the monomer measured here. Oligomers were modelled by allowing a 4 or 8 Å overlap between different subunits, giving a centre to centre distance of 36 or 32 Å respectively which is comparable to the most compact forms of the dimer measured here. Models were constructed by placing atoms 36 Å apart either in a sequential linear arrangement or by placing the centre of the sphere at the points of regular polygons in which the sides were 36 or 32 Å in length. The radius of the carbon atoms was set to 19.9 Å within the atomic radii library initially based on the AMBER-ff99 parameters [8] used by the projection approximation script. **Fig. S1** shows the hexagonal ring arrangement and associated pdb file text. The same structure with alternate of initial coordinates were generated and Ωs calculated to ensure that the high symmetry and precise

alignment to the axes of the coordinate system did not causing "eclipse" type states to arise such that one atom exactly obscured another. The compiled script is freely available from https://github.com/tumbling-cross-section
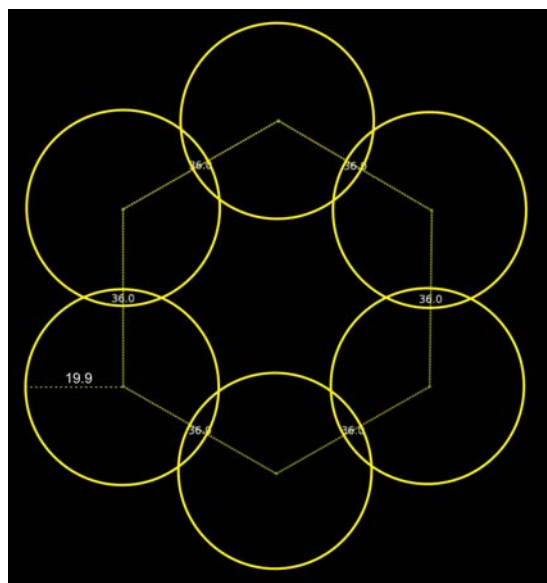

FIGURE S1 Ring like arrangement for a hexametric oligomer of α-syn. Atoms were placed at the corners of a regular hexagon spaced 36 Å apart. Each atom represented a compact monomer and was designated a radii of 19.9 Å allowing a 4 Å overlap between subunits. Measurements were taken using the PyMOL Molecular Graphics System. The pdb file that describes this structure is shown below.

```
ATOM    1 C01 ALA A  9    31.177  18.000  0.000 0.00 0.00    E   C
ATOM    1 C01 ALA A  9    31.177 -18.000  0.000 0.00 0.00    E   C
ATOM    1 C01 ALA A  9     0.000  36.000  0.000 0.00 0.00    E   C
ATOM    1 C01 ALA A  9   -31.177  18.000  0.000 0.00 0.00    E   C
ATOM    1 C01 ALA A  9   -31.177 -18.000  0.000 0.00 0.00    E   C
ATOM    1 C01 ALA A  9     0.000 -36.000  0.000 0.00 0.00    E   C
END
```
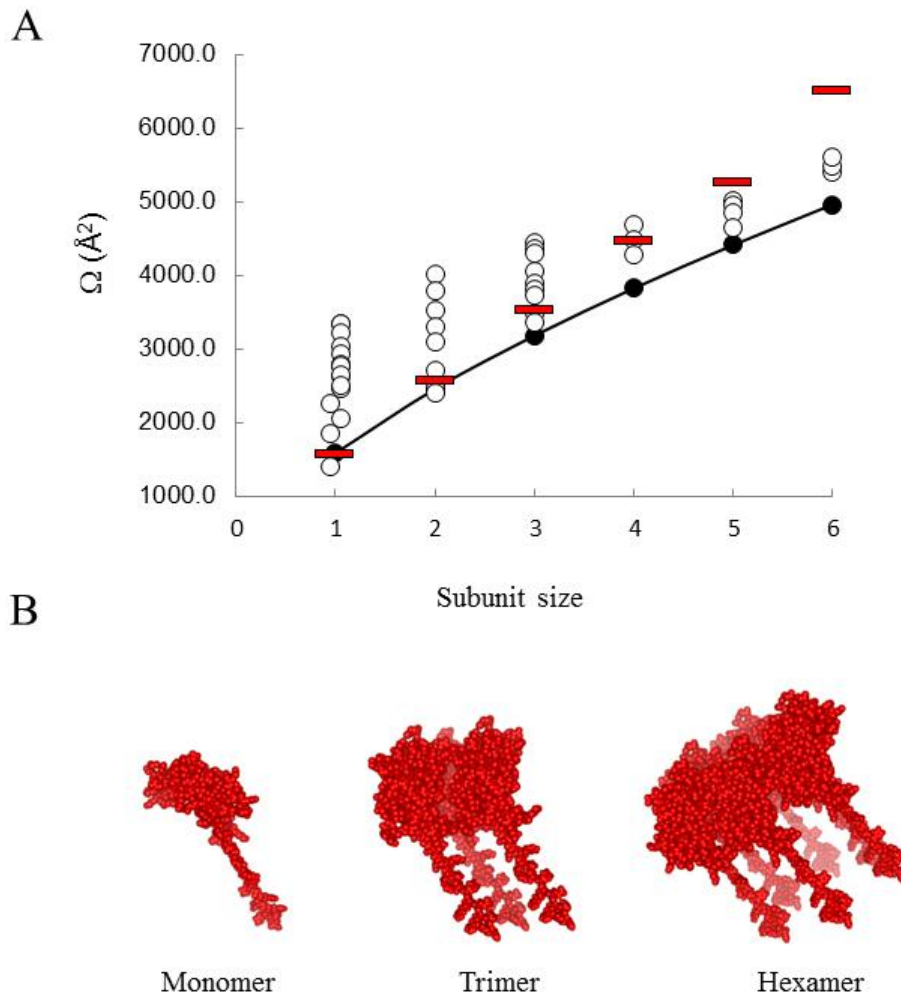
FIGURE S2 (A) Theoretical Ωs for a partially collapsed state of a 140 amino acid protein**.** Open circles, Ωs of each charge state ion according to oligomer size produced by protocol 1. Expected Ωs were calculated for a range molecular weights (MW) assuming a perfect sphere of density 0.37 Da$/$Å^3. Red lines represent the calculated Ωs for a partially collapsed state. The x axis is subunit size and the y axis shows Ω in Å^2. (B) Expected Ωs of model spherical structures with the same mass as the oligomers, based on the globular protein standards are shown as *black circles*. Models were constructed by taking the 100 amino acid protein beta-2 microglobulin (pdb - 1LDS) and including a 40 amino acid linear amino acid strand to the edge of the protein to model a partially folded state which consisted of a compact core and extended termini. Theoretical Ωs were obtained by a projection approximation algorithm as described before [4].
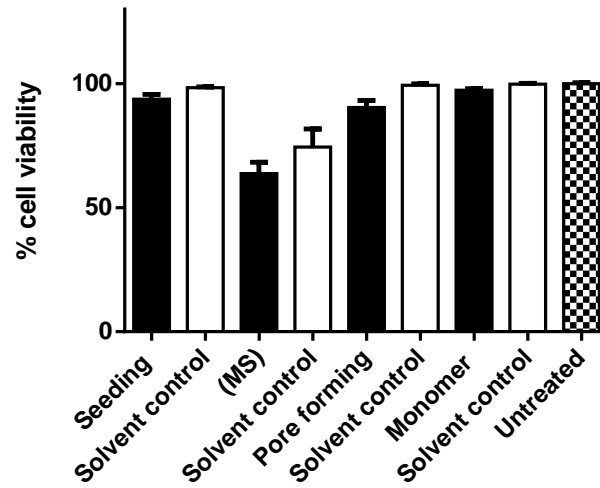
FIGURE S3 MTT viability assay was performed after 8 h treatment showed no significant loss in cell viability, indicating that Ca^{2+} influx was not a secondary effect of cell death. MTT cell viability assay of SH-SY5Y human neuroblastoma cells performed at $1.0x10^5$ cells/well seeding density after 8 h incubation with oligomers originating from seeding, pore forming protocols and MS compatible conditions, alongside with respective controls at 10% v/v. Means are plotted with ±SEM, values have been normalised to untreated cells (100%)

Supplementary Table 1

Protein	Mass (Da)	Ω (Å^2)	SD
bovine insulin	5734	760	±48
bovine ubiquitin	8565	1199	±65
equine cytochrome c	12355	1622	±94
bovine α-lactalbumin	14178	1533	±81
hen egg lysozyme	14305	1469	±60
horse heart myoglobin	17562	1971	±267
porcine elastase	25907	2134	±102
carbonic anhydrase	29090	2012	±186
ADH monomer	39804	3011	±74
albumin monomer	66463	4184	±300
ADH tetramer	159216	8497	±228
extended α-syn monomer	14460	2482	±159
compact α-syn monomer	14460	1851	±276
denatured α-syn monomer	14460	2620	±220
α-syn dimer	28920	3162	±604
α-syn trimer	43380	3940	±220
α-syn tetramer	57840	4489	±208
α-syn pentamer	72300	4868	±157
α-syn hexamer	86760	5498	±97

Table S1 Compiled experimentally determined Ωs of a range of model proteins under native conditions. The reported values are the mean Ω over all charge states of the proteins and standard deviations represent the spread in the recorded Ω across all charge states. All data was acquired on a Synapt G2 HDMS under the same conditions used to observe the α-syn oligomers. All values presented in Å^2.

α-syn	Mass (Da)	measured average		ring structure		partially collapsed	globular	linear
		Ω (Å^2)	SD	36 Å spacing	32 Å spacing			
denatured monomer	14460	2620	±220					
extended monomer	14460	2482	±159					
compact monomer	14460	1851	±276			1567	1584	
dimer	28920	3375	±751			2571	2450	2502
trimer	43380	3907	±232	3507		3520	3169	3701
tetramer	57840	4229	±225	4336		4467	3809	4654
pentamer	72300	4803	±167	5346	4758	5265	4394	5943
hexamer	86760	5553	±212	6316	5440	6513	4940	7034

Table S2 Compiled theoretically determined Ωs of a range of *in silico* model complexes. The reported experimental values are the mean Ω over all charge states of the proteins and standard deviations represent the spread in the recorded Ω across all charge states. Theoretical Ωs were obtained by a projection approximation algorithm as described before [4]. Ring-like and linear models were constructed by arranging spheres with a Ω comparable to the most compact state of the monomer. Theoretical Ωs for a spherical model were calculated assuming the monomer to be spherical structure with an average density of 0.37 Da/Å^3. Partially collapsed models were constructed by taking the 100 amino acid protein beta-2microglobulin (pdb - 1LDS) and including a 40 amino acid linear amino acid strand to the edge of the protein to model a partially folded state which consisted of a compact core and extended termini. All values presented in Å^2.

References

1 Smith, D.P., Tew, D.J., Hill, A.F., Bottomley, S.P., Masters, C.L., Barnham, K.J. and Cappai, R. (2008) Formation of a high affinity lipid-binding intermediate during the early aggregation phase of alpha-synuclein. *Biochemistry*. **47**, 1425-1434

2 Danzer, K.M., Haasen, D., Karow, A.R., Moussaud, S., Habeck, M., Giese, A., Kretzschmar, H., Hengerer, B. and Kostka, M. (2007) Different species of alpha-synuclein oligomers induce calcium influx and seeding. J.Neurosci. **27**, 9220-9232

3 Ruotolo, B.T., Benesch, J.L., Sandercock, A.M., Hyung, S.J. and Robinson, C.V. (2008) Ion mobility-mass spectrometry analysis of large protein complexes. Nat.Protoc. **3**, 1139-1152

4 Smith, D.P., Knapman, T.W., Campuzano, I., Malham, R.W., Berryman, J.T., Radford, S.E. and Ashcroft, A.E. (2009) Deciphering drift time measurements from travelling wave ion mobility spectrometry-mass spectrometry studies. Eur.J.Mass.Spectrom.(Chichester, Eng). **15**, 113-130

5 Smith, D.P., Radford, S.E. and Ashcroft, A.E. (2010) Elongated oligomers in beta2-microglobulin amyloid assembly revealed by ion mobility spectrometry-mass spectrometry. Proc.Natl.Acad.Sci.U.S.A. **107**, 6794-6798

6 Knapman, T.W., Berryman, J.T., Campuzano, I., Harris, S.A. and Ashcroft, A.E. (2010) Considerations in Experimental and Theoretical Collision Cross-section Measurements of Small Molecules Using Travelling Wave Ion Mobility Spectrometry-Mass Spectrometry. Int. J.Mass.Spec. **298**, 17-23

7 Gonzales, A. (2010) Measurement of areas on a sphere using Fibonacci and latitude-longitude lattices. Mathematical Geosciences. **42,** 49-64

8 Cornell, W., D., Cieplak, P., Bayly, C., I., Gould, I., R., Merz, K., M., Ferguson, D., M., Spellmeyer, D., C., Fox, T., Caldwell, J., W. and Kollman, P., A. (1995) A Second Generation Force Field for the Simulation of Proteins and Nucleic Acids. J. Am. Chem. Soc. **117**, 5179-5197